coatings

MDPI

Article

Metakaolin-Reinforced Sulfoaluminate-Cement-Solidified Wasteforms of Spent Radioactive Resins—Optimization by a Mixture Design

Jiaqian Xu, Mengzhou Wang, Cong Li, Mengxing Han, Qi Wang and Qina Sun *

Hebei Key Laboratory of Heavy Metal Deep-Remediation in Water and Resource Reuse, School of Environmental and Chemical Engineering, Yanshan University, Qinhuangdao 066004, China
* Correspondence: sunqn@ysu.edu.cn

Abstract: Cement solidification is a main technique for radioactive waste treatment to reduce its risk to the environment and human health. However, this method underperforms when dealing with spent radioactive ion-exchange resin, taking much space, and costing much money for final disposal. In this work, simulated spent radioactive resin was solidified using a metakaolin-reinforced sulfoaluminate cement system, which was optimized by a mixture design based on the effects of components and parameters, and the durability of solidified wasteforms was assessed in terms of strength and Cs(I) leaching. Solidified by an optimized formula of 40 wt.% spent resin, 55.8 wt.% sulfoaluminate cement, 2.2 wt.% metakaolin, and 2 wt.% water reducer, the resin loading in wasteforms reached 64% and the compressive strength 13.7 MPa. The dominant mineral phases of hydration products were ettringite crystalline of acicular and columnar morphology, with small amounts of scattered amorphous clusters of aluminum gels and C–S–H gels. Metakaolin, a source of aluminum, promoted the growth of ettringite, which facilitated (1) the encapsulation of resin beads with high strengths, even in acidic environments or during frequent freezing-thawing, and (2) the retention of Cs(I), with a 42 day leaching rate of 2.3×10^{-4} cm/day. This work offers a technical justification for spent resin solidification in the metakaolin-reinforced sulfoaluminate cement system, which is an applicational solution for the efficient treatment of radioactive waste.

Keywords: spent radioactive resin; cement solidification; sulfoaluminate cement; metakaolin; nuclides leaching; mixture design

check for updates

Citation: Xu, J.; Wang, M.; Li, C.; Han, M.; Wang, Q.; Sun, Q. Metakaolin-Reinforced Sulfoaluminate-Cement-Solidified Wasteforms of Spent Radioactive Resins—Optimization by a Mixture Design. *Coatings* **2022**, *12*, 1466. https://doi.org/10.3390/coatings12101466

Academic Editor: Maria Bignozzi

Received: 31 August 2022
Accepted: 29 September 2022
Published: 4 October 2022

Publisher's Note: MDPI stays neutral with regard to jurisdictional claims in published maps and institutional affiliations.

Copyright: © 2022 by the authors. Licensee MDPI, Basel, Switzerland. This article is an open access article distributed under the terms and conditions of the Creative Commons Attribution (CC BY) license (https://creativecommons.org/licenses/by/4.0/).

1. Introduction

Radioactive waste streams come from a wide range of sources, including the nuclear fuel cycle, nuclear technology utilization, and reactor accidents [1–3]. One of the commonly used purification processing for radioactive waste streams is ion exchange, in which nuclide ions are extracted from aqueous streams and enriched onto ion exchange resin beads [4–6]. When the ion exchange sites of resins are saturated with radionuclides, they lose purification capacity and are discharged from treatment columns, thus forming spent radioactive resins to be solidified and disposed of. Cement solidification, with the advantages of low cost, operability, and good radiation resistance of the solidified wasteforms, is currently the most widely used solidification technique for treating spent resin before final disposal [7–15]. New cement compositions besides ordinary Portland cement (OPC) offers fresh perspectives on radioactive waste solidification, especially for wastes that are challenging for OPC to solidify [16,17]. Sulfoaluminate cement (SAC) is one of the emerging cementitious materials produced by calcining limestone, bauxite, and gypsum in a certain composition ratio configuration at relatively low temperatures [7,18–21]. The clinker minerals of SAC are mainly anhydrous calcium sulfoaluminate ($3CaO{\cdot}3Al_2O_3{\cdot}CaSO_4$), dicalcium silicate ($2CaO{\cdot}SiO_2$), and iron phase [7,18,20]. After blending the binder with water, hydration products of hydrated calcium sulfoaluminate (ettringite, $3CaO{\cdot}Al_2O_3{\cdot}3CaSO_4{\cdot}32H_2O$),

aluminum gel ($Al_2O_3 \cdot nH_2O$), and hydrated calcium silicate hydrate gels (C–S–H gels) generate early strength, frozen resistance, and impermeability, etc. Radioactive wastes, such as filter cartridges from gas purification, membranes, and evaporator concentrates from liquids treatment, are solidified by SAC and the wasteforms exhibit high compressive strengths and good resistance to immersion, indicating SAC as being a promising cementitious material for radioactive waste treatment and disposal [7,20,22–24].

However, similar to OPC, the biggest problem with spent resin wasteforms solidified by SAC is that they cannot withstand prolonged water immersion [21,25,26]. This is because, during the curing process, the water in the wet resin is thoroughly customed in the hydration reaction, thus reducing the diameter of the resin beads and encapsulating them in a comparable size cavity. When the wasteforms are subjected to prolonged water immersion, water enters through the pores of wasteforms, the resin absorbs water, and the beads swell and become larger in diameter, thus generating static pressure on the cavity walls [5]. With volume loadings of resin in the wasteforms of 30%~40%, it may cause the wasteforms to crack, thus making it easier for water to penetrate [7]. Resin swelling force and water chemistry result in the wasteforms breaking and disintegrating. In this case, free nuclide ions may migrate into the water; broken fragments and dislodged resin beads may also diffuse, causing radioactive contamination. To overcome this drawback, researchers have investigated many approaches, such as reducing the resin loadings and wrapping the wasteforms with hydrophobic film, which increases the waste to be disposed of and the process complexity [7].

Metakaolin ($Al_2O_3 \cdot 2SiO_2 \cdot 2H_2O$) is a typical clay material with the main components of SiO_2 and Al_2O_3; Al_2O_3 content is 40% and more, which is higher than other clay minerals [27–30]. Commercial metakaolin is produced by kaolinite calcination at a temperature of 600~800 °C [28,30,31]. The crystalline kaolinite is mainly in irregular squamous sheets bonded by Van der Waals bonds. By calcination, the lamellar structure of kaolinite remains unchanged, but the crystal size decreases [28,31]. Meanwhile, the particle gap reduces, forming metakaolin with a poorly crystallized transition phase with more agglomerated particles [27,29]. The formation of unsaturated ligands during calcination derives a thermodynamically metastable state of metakaolin, which possesses a high-pozzolanic reactivity as an artificial cementitious additive for cements [27,32–34]. Pozzolanic reaction of metakaolin occurs at the early stage of cement hydration, thus promoting the early hydration of clinker minerals, shortening the hydration induction period and early hydration acceleration period of medium- and low-heat Portland cement [31,32]. Afterwards, the ongoing pozzolanic reaction substantially increases hydration products as the secondary hydration reaction, in which the active aluminum component participates and generates C–S–H gels [33]. Moreover, the ultra-fine metakaolin powder fills the pores, decreases pore size, and reduces the total pore volume and porosity [31,32]. These reactions and effects lead to a denser microstructure and higher mechanical properties of the hardened cement [31–33,35]. Because of these advantages for cement mechanics, metakaolin has been widely used in the construction industry; therefore, it is reasonable to expect that metakaolin will play a beneficial role in solidifying radioactive wastes. However, metakaolin has been less studied as a solidification additive for radioactive waste treatment. The performance of metakaolin-reinforced solidification of spent resins in sulfoaluminate cementitious systems has never been reported.

In order to improve the performance of solidification of spent radioactive resins, in this work, we solidified simulated spent resin using a metakaolin-reinforced sulfoaluminate cementitious system and investigated the effects of solidifying components and parameters on the wasteforms. The solidification was optimized by a mixture design to improve the comprehensive performance of wasteforms, including compressive strength, durability, and nuclide leaching property. The microscopic morphology and hydration products of the cured bodies were characterized by SEM and XRD to analyze the curing mechanism of the metakaolin-reinforced sulfoaluminate cement system.

2. Materials and Methods

2.1. Materials

Sulfoaluminate cement was purchased from Polar Bear Special Cement Co., Tangshan, China, and the main mineral components are anhydrous calcium sulfoaluminate ($3CaO{\cdot}3Al_2O_3{\cdot}CaSO_4$), dicalcium silicate ($2CaO{\cdot}SiO_2$), and $CaSO_4$ and $CaCO_3$ blended during production (Figure S1, see Supplementary Materials). Metakaolin and naphthalenesulfonate water reducer were purchased from Beichen Admixture Co., Tianjin, China. Cesium nitrate (A.R.) was purchased from Kaitong Chemical Reagent Co., Tianjin, China. Polystyrene ion exchange resin was offered by Zhengguang Resin Co., Zhejiang, China, and the main composition and total exchange capacity are listed in Table S1. Simulated radioactive resins were prepared by immersing polystyrene ion-exchange spent resin in cesium nitrate solution and stirring continuously for 48 h to ensure adsorption equilibrium for Cs(I). Afterwards, the wet resin with a water content of 68.8% was solidified as the simulated resin without further treatment.

2.2. Solidification and Performance Tests

A typical out-of-vessel mixing method is used for the solidification operation [23,36]. The sulfoaluminate cement, metakaolin, and naphthalenesulfonate water reducer were put to the vessel and mixed at low speed. Then the simulated spent resin is added, and all materials are stirred into a well-mixed paste. The paste was slowly injected into Ø50 mm × 50 mm cylindrical molds and tapped to discharge large air bubbles. The upper surface was scraped and then cured at 25 ± 5 °C with relative humidity ≥ 90%.

The effects of metakaolin, spent resin loadings in wasteforms, water-binder (w/b) ratios, and water reducer dosages on the solidification performance were investigated by the controlled variable method. The compressive strength of demolded wasteforms was tested after 7 days curing on a fully automatic pressure tester (SY-200, Jinan Testing Machine Co., Jinan, China), and the arithmetic mean from four parallel samples was used for further assessment. The initial and final setting times of the wasteforms were determined using the Vicat needle test by a Vicat apparatus (ISO standard, Wuxi Construction Instrument and Material Machinery Co., Wuxi, China), according to the Chinese Standard GB/T 1346-2011. The fluidities were measured in accordance with the Chinese Standard GB/T 2419-2005 based on the spread diameter in a cone test, using a cement mortar fluidity tester (NLD-3, Zhongluda Instrument Technology Co., Tianjin, China).

2.3. Solidification Optimization by Mixture Design

A mixture design was employed to optimize the solidification of spent resin in metakaolin-reinforced cement. The factors in the mixture design, denoted as X_i, are the components of a cementitious system with the constraints shown in Equation (1) [37–39],

$$\begin{cases} \sum_{i=1}^{n} X_i = 1 \\ a_i \leq X_i \leq b_i \end{cases} \quad (1)$$

where, a_i and b_i are the lower and upper limits of factor X_i, respectively.

Fluidity, resin loading by volume, final setting time, and 7 day compressive strength are the responses, noted as Y_1, Y_2, Y_3, and Y_4, respectively. A quadratic polynomial model including only primary and interaction terms is used to describe the relationship between the response values and the factors, and to predict and optimize the response values, as shown in Equation (2) [37–40]. The experiments were arranged by the software Design Expert, the results were analyzed, and the model regression coefficients were computed. The multiobjective optimization was performed using the satisfaction function method [37,41].

$$Y = \sum_{i=1}^{n} \beta_i X_i + \sum_{i=1}^{n-1} \beta_{ij} X_i X_j \ (1 \leqq \mathrm{i} \leqq \mathrm{n}, \quad j = i + 1) \quad (2)$$

2.4. Solidified Wasteforms Durability Tests

Solidified wasteforms durability tests include evaluation of compressive strength loss after immersion or freeze–thaw cycles and Cs(I) leaching behavior [23]. Compressive strength as control was measured after 28 days of curing. In the immersion tests, solidified samples were immersed in deionized water without pH adjustment at 25 ± 5 °C for 30 days, 90 days and 180 days, respectively, and different pHs of 3, 5, 7, 9, and 11 were used in the 90 day immersion. The change in compressive strength before and after immersion was used to evaluate the strength loss. In a freeze–thaw cycle, the cured bodies were frozen at −20 °C for three hours and thawed at 20 °C for four hours [42]. The samples were evaluated for strength loss after undergoing an infinitesimal number of cycles.

The Cs(I) leaching test was conducted using semidynamic experimental methods with reference to the Chinese National Standard GB7023-1986 [23,42]. The mass of cesium contained in each standard curing body was 66.14 mg. Deionized water 1.6 L at 25 ± 5 °C at different pH was used as the leachant, and the ratio of leachant volume to the surface area of the waste form V_L/F was 13.35. After the 1st, 3rd, 7th, 10th, 14th, 21st, 28th, 35th and 42nd days of leaching, the deionized water was replaced. The mass of Cs(I) in the leachant was calculated from Cs(I) concentration that was determined by an atomic absorption spectrophotometer (TAS-990 AFG, PuXi General Instrument Co., Beijing, China).

The leaching rate R and cumulative leaching fraction P are determined in a semidynamic leaching test and calculated from the mass of Cs(I) leached into the leachant from the wasteform, as shown in Equations (3) and (4), respectively [8,23,42],

$$R_n = \frac{a_n / A_0}{F/V} \cdot \frac{1}{t_n} \tag{3}$$

$$P_t = \frac{\sum a_n / A_0}{F/V} \tag{4}$$

where t is the durative days of immersion, d, $t = \Sigma t_n$, and in the nth interval of t_n days, the leaching rate and leached mass of Cs(I) are R_n, cm/day, and a_n, g, respectively; A_0 is the average initial Cs(I) mass in a sample, 66.14 mg in this case; F is the surface area of a sample, cm^2; V is the volume of a sample, cm^3; P_t is the cumulative fraction leached of Cs(I) on the tth day, cm.

2.5. Characterization of Solidified Wasteforms

The morphology and mineral phases of the hydration products of the solidified wasteforms were characterized and analyzed by scanning electron microscopy (FESEM, S-4800, Hitachi, Tokyo, Japan) and X-ray diffraction (XRD, D/max 2550 PC, Rigaku, Tokyo, Japan). The samples were crushed and ground, immersed in anhydrous ethanol to terminate the hydration, and dried. The SEM samples were observed after plating with gold films. XRD analysis was performed using samples ground to fine powders with a scan speed of 7° 2θ/min, step size of 0.02°, and a scan range of 5° to 70° 2θ.

3. Results and Discussion

3.1. Factors Affecting the Solidification Performance

The effects of metakaolin, spent resin loadings in wasteforms, water-binder (w/b) ratios, and water reducer dosages on the solidification performance were investigated and the results are shown in Figure 1. Metakaolin dosage is the major concerning factor (Figure 1a) for its pozzolanic reactivity. The 7 day compressive strength increased with the increase in metakaolin dosage, indicating that the secondary hydration of the metakaolin improved the microstructure and then enhanced the mechanical properties and durability of the solidified wasteforms at the macroscopic level [30]. At the same time, metakaolin reduced the fluidity significantly and shortened both the initial and final setting times of the paste. The trends of strength, fluidity, and setting times indicate that metakaolin boosted the hydration reaction rate of the sulfoaluminate cementitious system to facilitate the

solidification. In terms of operating parameters, with no metakaolin addition, the fluidity reached 300 mm, which makes the resin beads subject to a decreasing fluid resistance in the paste and keep floating up and gathering in the upper part of the paste. The floating resin beads were delaminated with the cement during a period around 100 min before the initial setting, which is one of the reasons for the low compressive strength in this case. Owing to appropriate metakaolin dosages, it was also facile to blend the paste uniformly and fill the mold without large bubbles with fluidity between 150 mm and 200 mm, which meets the needs of solidifying procedures. The setting times for paste containing metakaolin were also within a reasonably acceptable range, with the initial setting time for sufficient stirring being no less than 40 min and the final setting time for minimizing delay on subsequent processing steps and personnel exposure risk being no more than 90 min.

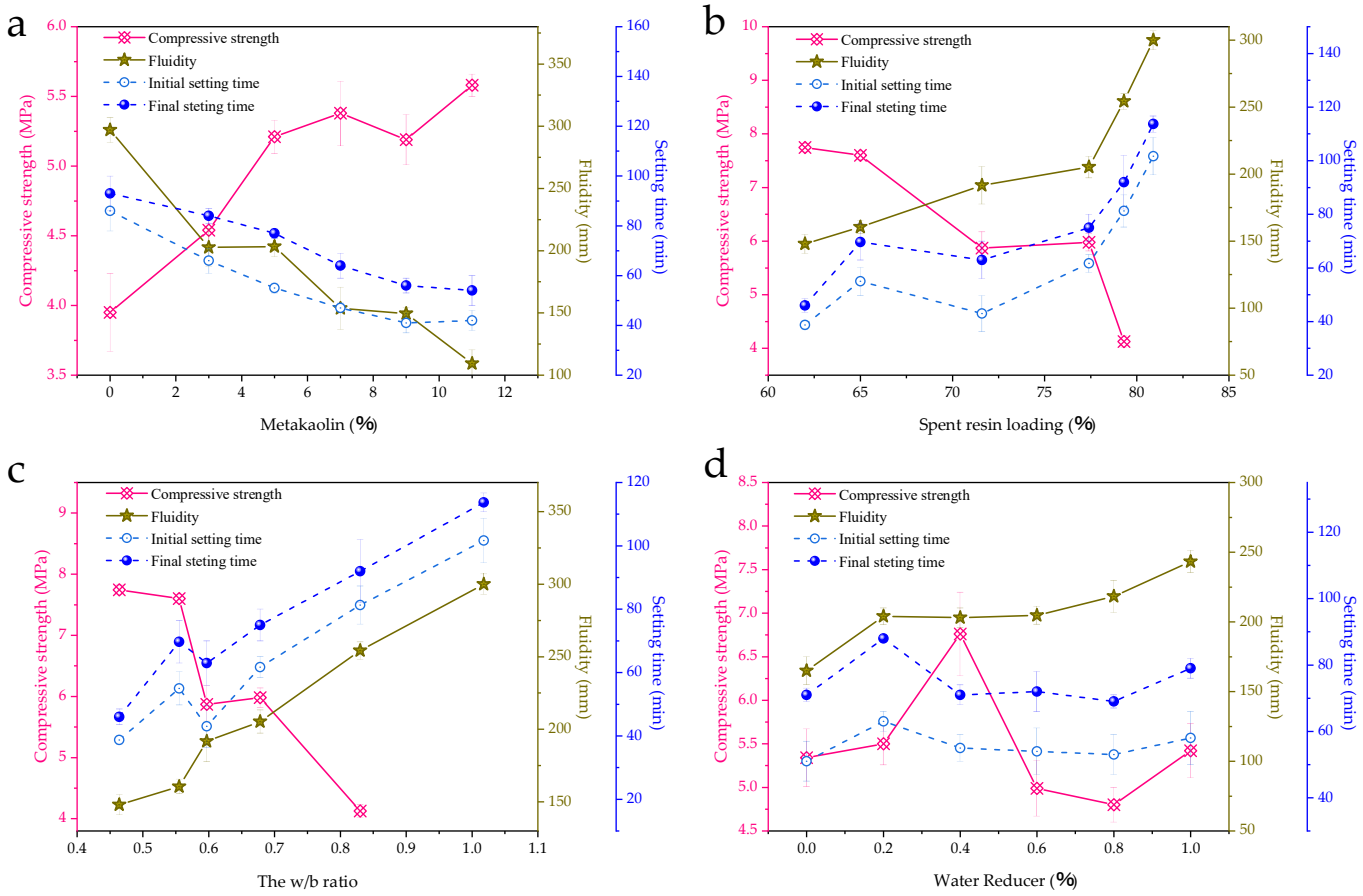

Figure 1. Solidification performance affected by (**a**) metakaolin (spent resin loading 77.4%, w/b ratio 0.68, water reducer 0.4%), (**b**) resin loading (metakaolin 5%, water reducer 0.6%~0.7%), (**c**) w/b ratio (metakaolin 5%, water reducer 0.6%~0.7%), and (**d**) water reducer (metakaolin 5%, spent resin loading 77.4%, w/b ratio 0.68).

Generally speaking, more resin added in the solidification system results in a larger resin loading in the final wasteforms, despite cementitious components affecting the composition of hydration products and the pore structure of the solidified wasteforms, resulting in differences in their volumes [25]. More practically, resin loading indicates whether the smallest waste package is formed for the same resin volume [21]. Therefore, resin loading is used as an indicator to examine the effects of spent resins on solidifying performance, as shown in Figure 1b. With increased resin loading, the wasteforms' compressive strength fell noticeably and rapidly, reaching ~5.8 MPa with a loading higher than 70%. High resin loadings also resulted in more free water and, therefore, caused an increase in fluidity and prolonged setting times. There was a modest rise in fluidity with a 64% loading, but when

the loading was increased to 80%, the fluidity increased to 300 mm, and the resin floated up, which was one of the causes of the low compressive strength. To further illustrate the role of free water in the system, extra water was added in addition to the 68.8% water contained in the resin. The w/b ratio effects on the solidifying performance are shown in Figure 1c. The w/b ratio curve resembles the spent resin loading curve. The fluidity increased almost linearly with increasing w/c ratios. Although it benefited the operation, the excess water in the system over that required for the hydration reaction greatly retarded the solidification. Thus, there is a noticeable decline in the compressive strength curve. Therefore, water reducers providing additional fluidity without introducing excess water are essential for solidification. In the experimental range (Figure 1d), the water reducer increased the fluidity well, without drastically weakening both setting times and compressive strength. This is due to the effect of naphthalenesulfonate on the dispersion and surface lubrication of binder particles [43,44].

Through controlled variable experiments, we determined the effectiveness of metakaolin on the reinforcement of sulfoaluminate cement systems. We set a reasonable range of solidifying components based on the results in Figure 1, as shown in Table 1, for optimizing the overall performance of the solidified wasteforms through a mixture design.

Table 1. Upper and lower limits of factors.

Factors	Components	a_i (wt.%)	b_i (wt.%)
X_1	Spent resin	35	48
X_2	Sulfoaluminate cement	47	57.8
X_3	Metakaolin	2.2	5.9
X_4	Naphthalenesulfonate water reducer	2	2.5

3.2. Mixture Design Optimization

A $p = 4$ mixture design was performed with factors in Table 1 using the software Design Expert. The experimental runs were arranged, and the responses were 7 day compressive strength, final setting time, fluidity, and resin loading, as shown in Table S2. The data in Table 2 were fitted by the quadratic polynomial model of Equation (2), and the fitting coefficients were computed (Table S3). The model fitness assessment and analysis of variances results are presented in Table 2 and Table S4, respectively. The fluidities exceeded the 300 mm measuring range in runs 2 and 6 and were not measured; hence, they were removed from the fitting of Y_3. Runs 2, 3, 5, and 6 failed to record specific compressive strengths due to resin uplift and delamination, and these results were disregarded for fitting Y_1.

Table 2. Model fitness for responses.

Responses	R^2	R^2_{adj}	R^2_{pred}	S/N
Y_1	0.8588	0.8323	0.788	16.237
Y_2	0.9099	0.8289	0.809	10.521
Y_3	0.9652	0.9338	0.6735	15.745
Y_4	0.9478	0.938	0.9203	28.725

For each response in Table 2, both the coefficients of determination R^2 and the adjusted coefficients of determination R^2_{adj} show that the model's predictions and the experimental data match well [37,38]. This is notably evident for the responses Y_3 and Y_4. The experimental data were well-predicted by the model since the coefficients of determination for the prediction, R^2_{pred}, were quite close to R^2_{adj} [37,38]. The lowest signal-to-noise ratio S/N of the regressions was 10.521 (Y_2). All the $Pr > F$ values of the four fittings in the ANOVA (Table S4) were less than 0.0004, the lack-of-fit terms were all insignificant, and

the fitting results were free of outliers, demonstrating that the model significantly fit the experimental data [45]. The model fitness assessment and analysis of variances results suggest that the quadratic polynomial model in Equation (2) is valid for regression analysis and prediction of the experimental data of simulated spent-radioactive-resin solidification by metakaolin-reinforced sulfoaluminate cement.

Based on the quadratic polynomial model, multi-objective optimization using the satisfaction function for solidification was conducted to enhance the overall performance of the solidified wasteforms [37]. The optimized mixture composition, model predictions, and validation experiment data are listed in Table 3. The experimental data of this optimized solidification formula matched the predicted values, and a w/b ratio of 0.445 provided smooth solidifying operation, high resin loading, and compressive strength of the wasteforms.

Table 3. Optimized mixture composition and results of prediction and validation experiments.

Mixture Composition (wt.%)				Predicted Responses				Experimental Data			
X_1	X_2	X_3	X_4	$Y_{1'}$ (MPa)	$Y_{2'}$ (min)	$Y_{3'}$ (mm)	$Y_{4'}$ (%)	Y_1 (MPa)	Y_2 (min)	Y_3 (mm)	Y_4 (%)
40	55.8	2.2	2	9.93	66.14	232.8	73.23	11.6	70	227	64

3.3. Durability of Solidified Wasteforms

After 28 days of curing, the optimized wasteforms were tested by immersion and freeze–thaw cycles, and the compressive strengths are depicted in Figure 2. The compressive strength did not reduce after being immersed in deionized water for 30, 90, or 180 days; rather, it increased by 6.3% to 15.6% compared to the control (Figure 2a). The sulfoaluminate cement continued to hydrate for 30 to 180 days in the water, ensuring the mechanical stability and resin beads sequestration in the wasteforms with a 64% resin loading. Whereas the pH of the immersion system impacted the durability of the wasteforms. Figure 2b shows that 90 days of immersion in neutral and alkaline systems increased compressive strength, while acidic systems with pHs of 3 and 5 significantly decreased compressive strength by 21.3% and 15.7%, respectively. This is because the sulfoaluminate hydration products disintegrated in acid media, weakening the strengths [21,46]. However, it is noteworthy that the compressive strength was 10.79 MPa, which is still higher than the 7 MPa required by the Chinese national standard GB14569.1-201 [42] for wasteforms to enter the final disposal sites, even after 90 days of immersion under unfavorable conditions at pH = 3. On the other hand, the durability was more negatively impacted by the repeated freeze–thaw cycles than by immersion. After 5 freeze–thaw cycles, the compressive strength was dramatically reduced with a loss of 16.7% before leveling off, while 20 cycles resulted in a 24.3% strength reduction. The optimized wasteforms performed better than the GB14569.1-2011 demands during freeze–thaw cycles, losing no more than 25% of their strength over five cycles. Additionally, their property satisfied practical applications because the permafrost layer thickness is typically taken into account when choosing disposal sites, preventing frequent freeze–thaw alternation of wasteforms [47–49].

The leaching behavior of typical nuclide Cs at different pHs was further investigated because of the significant effect of immersing pH on the strength of wasteforms. Nonradioactive isotopes were used instead of the radionuclide ^{137}Cs since they are chemically equivalent in solution [50]. Figure 3 shows the trends of leaching rate R and cumulative leached fraction P changes of Cs(I) in 42 days of leaching experiments, which exhibit similar trends at all pHs. R decreased with prolonged leaching time, while P increased; however, the extents of R and P altered at different stages. The initial 10 days corresponded to the rapid leaching phase of Cs(I). On the 10th day, P reached 42.5–46.8% of the total P for 42 days, while R reached a high order of magnitude of 10^{-2} cm/day. After that, the leaching of Cs(I) slowed down significantly, R stabilized at 10^{-3} and 10^{-4} cm/day orders of magnitude, and P accumulated the remaining ~50% during the following 32 days. R and P were not significantly affected by the varied pH values, notably pH = 3 and pH = 5,

implying that the solidified package sequestered Cs(I) effectively in the acidic leaching solution. The highest *P* of 0.467 cm was observed under the alkaline condition of pH = 11, not considerably different from 0.416 cm at pH = 3, which was also related to the fact that Cs(I) is soluble as CsOH at alkalinity [50,51]. These results suggest that the solidified wasteforms can wrap the resin particles to maintain the whole with high resin loadings and sequester the soluble cations in a strongly acidic environment, effectively preventing the radionuclides from diffusing into and further migrating in the environment.

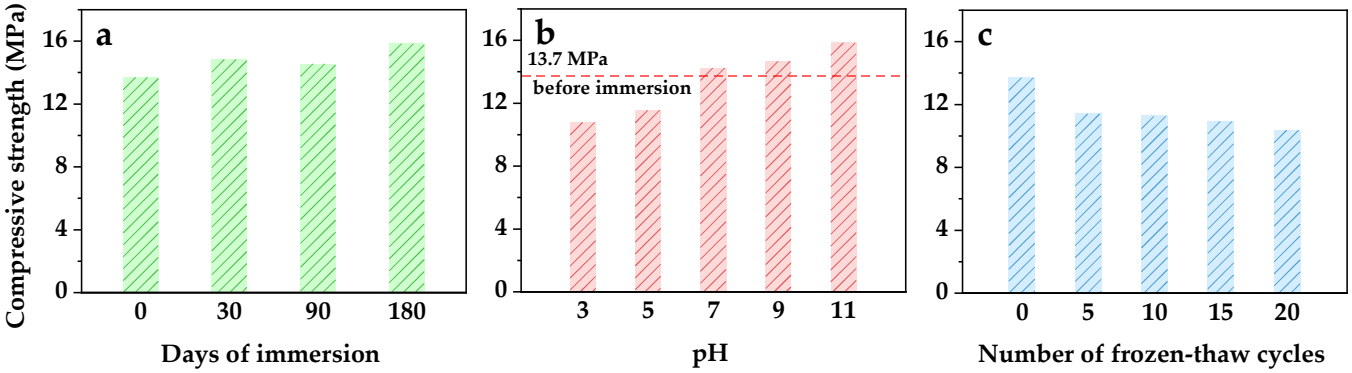

Figure 2. Compressive strength of optimized solidified wasteforms after (**a**) immersion of different days (pH = 7, 25 ± 5 °C), (**b**) 90 day immersion under different pH (25 ± 5 °C), and (**c**) freeze–thaw cycles, with the mixture composition of spent resin 40 wt.%, sulfoaluminate cement 55.8 wt.%, metakaolin 2.2 wt.%, and naphthalenesulfonate water reducer 2 wt.%.

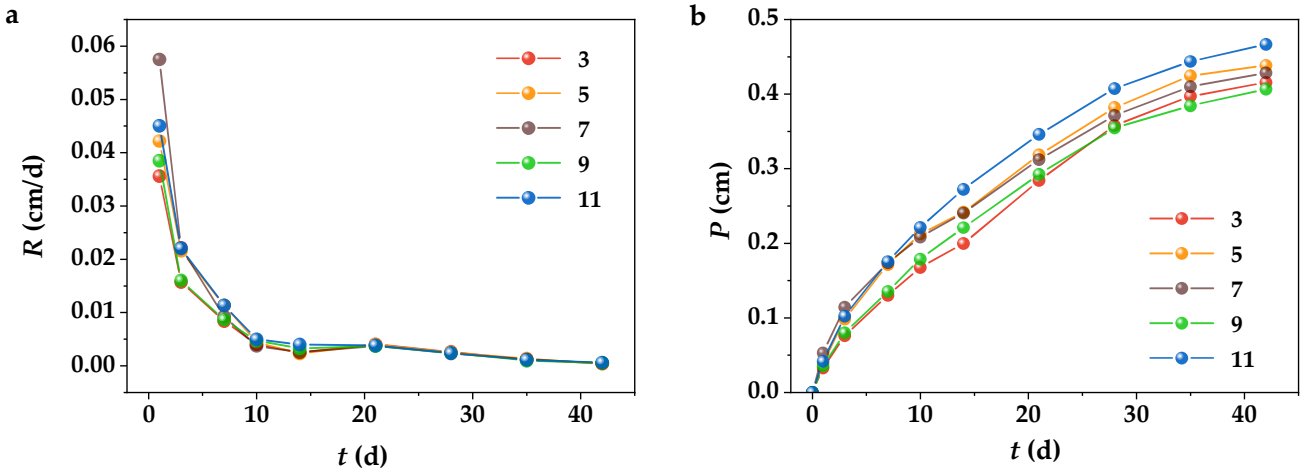

Figure 3. Leaching behavior of the simulated nuclide Cs^+: (**a**) Leaching rates and (**b**) cumulative leaching fractions; V_L = 1.6 L, V_L/F = 13.35, 25 ± 5 °C.

3.4. Hydration Products of Metakaolin-Reinforced Wasteforms

The encapsulation of resins in the metakaolin-reinforced wasteforms depends on its hydration products. The SEM images and XRD spectra in Figure 4 reveal the microscopic morphology and mineral content of the hydration products after 28 days of curing. As seen in Figure 4a, a stable crystalline skeletal structure scattered with amorphous products is formed by many acicular and columnar crystals interspersed throughout. The active ingredients in the sulfoaluminate clinker, such as anhydrous calcium thiosulfate, calcium aluminate, and dicalcium silicate, react when the cement comes into contact with water to create ettringite and C–S–H gels [19,20,52]. Following the abovementioned reactions, the generated $Ca(OH)_2$ interacts with calcium sulfate and aluminum gels to produce calcium alumina (Equation (5)) [51]. The basic structural unit of ettringite is $\{Ca_3[Al(OH)_6]\cdot 12H_2O\}^{3+}$, which belongs to the tripartite crystal system and presents the

typical columnar structure in Figure 4a [18,21,53–56]. This microstructure also supports the effect of metakaolin dosage on the wasteform performance in Figure 1a. On the one hand, Cs(I) retention in the wasteforms derived from Cs(I) immobilization in the mineral lattice of fully grown ettringite crystalline. On the other hand, the integrity and durability of the optimized wasteforms through the response surface methodology contributed to the physical encapsulating of radioactive wastes.

$$3Ca(OH)_2 + 3CaSO_4 + Al_2O_3 \cdot 3H_2O + 26H_2O \rightarrow 3CaO \cdot Al_2O_3 \cdot 3CaSO_4 \cdot 32H_2O \quad (5)$$

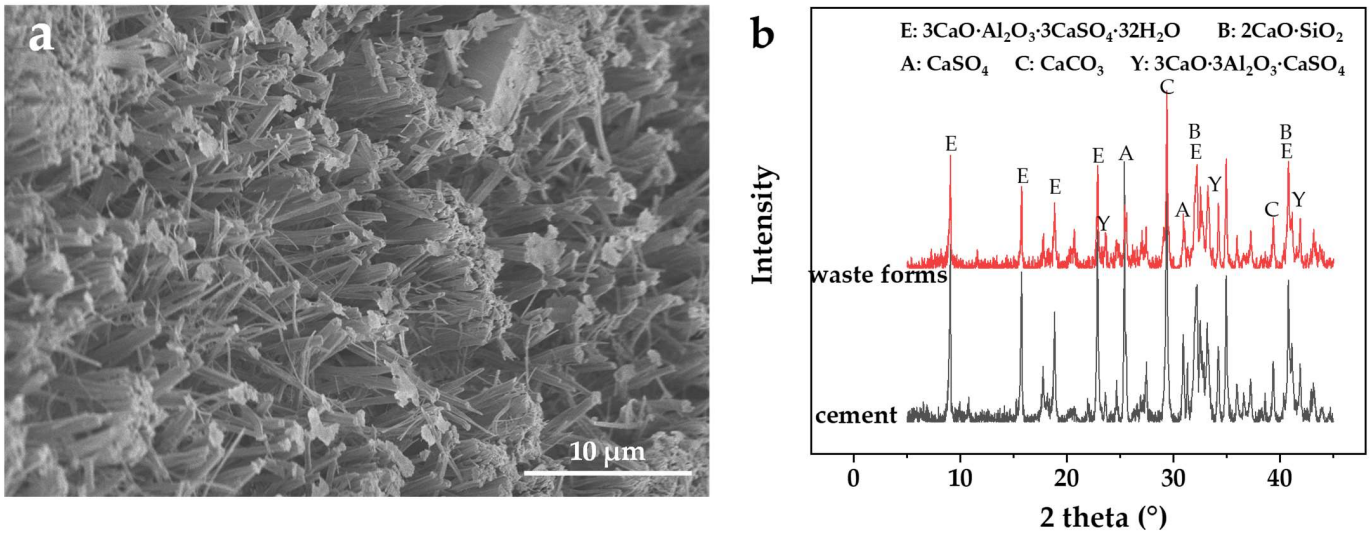

Figure 4. Characterization of metakaolin-reinforced wasteforms: (**a**) SEM image and (**b**) XRD spectra (red), with the mixture composition of spent resin 40 wt.%, sulfoaluminate cement 55.8 wt.%, metakaolin 2.2 wt.%, and naphthalenesulfonate water reducer 2 wt.%; the hardened cement XRD spectra (black) as comparison, with the mixture composition of water 40 wt.%, sulfoaluminate cement 55.8 wt.%, metakaolin 2.2 wt.%, and naphthalenesulfonate water reducer 2 wt.%.

Moreover, in the sulfoaluminate cementitious system reinforced by metakaolin, the amorphous Al_2O_3 in thermodynamically metastable metakaolin is very easily dissolved in an alkaline environment, which further offers the aluminum supply for hydration in Equation (5), in addition to the aluminum gels from sulfoaluminate clinker [27,29–32]. As a result, the reaction of Equation (5) and the creation of ettringite were both promoted, and the microstructure of the solidified wasteforms was strengthened. Furthermore, the amorphous products in Figure 4a are mainly C–S–H gels, aluminum gels, and some residual clinkers that were not entirely hydrated [23,25,26].

These hydration products exhibit characteristic peaks in the XRD spectra of wasteforms (red) and harden cement samples (black) without resins in Figure 4b, further qualitatively demonstrating that the mineral composition of hydration products was mainly ettringite, aluminum gels, and a small amount of C–S–H gels.

4. Conclusions

Metakaolin is a commonly used additive to improve the performance of cement in the construction industry and is a developing assistant in cementitious systems to solidify radioactive wastes. In this work, metakaolin was used to reinforce the sulfoaluminate-cement solidification of simulated spent radioactive resins, and the overall performance of the solidified wasteforms was optimized by the mixture design. With a high content of pozzolanic-reactive Al_2O_3, metakaolin facilitated the hydration of sulfoaluminate cement. The reinforced wasteforms, with a resin loading of 64%, met the disposal standards of GB14569.1-2011 for a compressive strength of 13.71 Mpa and the immersion and freeze–

thaw resistances. The wasteforms exhibited a good retention ability of Cs^+. The microscopic morphology was acicular and columnar crystals interspersed with amorphous gels and particles. Ettringite, aluminum gels, and C–S–H gels comprised the bulk of the mineral phases of the hydration products. The simulated spent radioactive resin was successfully solidified by the metakaolin-reinforced sulfoaluminate cementitious system, providing new insights into the safe treatment and disposal of radioactive wastes.

Supplementary Materials: The following supporting information can be downloaded at: https://www.mdpi.com/article/10.3390/coatings12101466/s1. Figure S1: Main mineral components of the sulfoaluminate cement used in the solidification experiment; Table S1: Main composition and property of the ion exchange resin used in the solidification experiment; Table S2: Mixture design and experimental data; Table S3: Regression model coefficients; Table S4: ANOVA results of the regression model.

Author Contributions: Writing—original draft preparation, J.X.; visualization, M.W.; methodology and validation, C.L.; investigation, M.H.; software and data curation, Q.W.; supervision and writing—reviewing and editing, Q.S. All authors have read and agreed to the published version of the manuscript.

Funding: This work was financially supported by the National Natural Science Foundation of China (No. 21301151), the Natural Science Foundation of Hebei Province (No. B2021203036 and No. B2018203331), and the University Science and technology Research Projects of Hebei Province (No. ZD2021103).

Institutional Review Board Statement: Not applicable.

Informed Consent Statement: Not applicable.

Data Availability Statement: Data sharing is not applicable to this article.

Conflicts of Interest: The authors declare no conflict of interest.

References

1. Burns, P.C.; Ewing, R.C.; Navrotsky, A. Nuclear fuel in a reactor accident. *Science* **2012**, *335*, 1184–1188. [CrossRef] [PubMed]
2. Wang, J.L.; Liu, X.J. Forward osmosis technology for water treatment: Recent advances and future perspectives. *J. Clean. Prod.* **2021**, *280*, 124354. [CrossRef]
3. Zhang, X.Y.; Gu, P.; Liu, Y. Decontamination of radioactive wastewater: State of the art and challenges forward. *Chemosphere* **2019**, *215*, 543–553. [CrossRef]
4. Wang, Z.; Guo, S.; Wu, Z.; Fan, H.; Guan, G.; Hao, X. A smart potential-responsive ion exchange nanomaterial with superparamagnetism for cesium ion separation and recovery. *Sep. Purif. Technol.* **2017**, *187*, 199–206. [CrossRef]
5. Wang, J.; Wan, Z. Treatment and disposal of spent radioactive ion-exchange resins produced in the nuclear industry. *Prog. Nucl. Energy* **2015**, *78*, 47–55. [CrossRef]
6. Rao, S.V.; Mani, A.G.; Karua, S.; Cheralathan, M.; Reddy, A.; Khandelwal, S.K.; Paul, B. Treatment of liquid wastes using composite resins. *J. Radioanal. Nucl. Chem.* **2016**, *307*, 463–469. [CrossRef]
7. Li, J.; Chen, L.; Wang, J. Solidification of radioactive wastes by cement-based materials. *Prog. Nucl. Energy* **2021**, *141*, 103957. [CrossRef]
8. Eskander, S.B.; Bayoumi, T.A.; Saleh, H.M. Leaching behavior of cement-natural clay composite incorporating real spent radioactive liquid scintillator. *Prog. Nucl. Energy* **2013**, *67*, 1–6. [CrossRef]
9. García-Gutiérrez, M.; Missana, T.; Mingarro, M.; Morejón, J.; Cormenzana, J.L. Cesium diffusion in mortars from different cements used in radioactive waste repositories. *Appl. Geochem.* **2018**, *98*, 10–16. [CrossRef]
10. Rakhimova, N.R.; Rakhimov, R.Z.; Morozov, V.P.; Potapova, L.I.; Osin, Y.N. Mechanism of solidification of simulated borate liquid wastes with sodium silicate activated slag cements. *J. Clean. Prod.* **2017**, *149*, 60–69. [CrossRef]
11. Deneanu, N.; Dulama, M.; Baboescu, E.; Teoreanu, I. The conditioning in Portland cement of oil radioactive wastes. *Rev. Chim.* **2004**, *55*, 966–970.
12. Lanier, S.; Davy, C.A.; Albert-Mercier, C.; Farcy, O.; Cau-Dit-Coumes, C.; Lambertin, D. Novel Portland cement matrices incorporating a gamma -MnO_2/Ag_2O hydrogen/tritium getter -structure changes and trapping performance. *J. Nucl. Mater.* **2022**, *567*, 153819. [CrossRef]
13. Phillip, E.; Khoo, K.S.; Yusof, M.A.; Rahman, R.O. Mechanistic insights into the dynamics of radionuclides retention in evolved POFA-OPC and OPC barriers in radioactive waste disposal. *Chem. Eng. J.* **2022**, *437*, 135423. [CrossRef]
14. Shaaban, I.; Assi, N. Measurement of the leaching rate of radionuclide Cs-134 from the solidified radioactive sources in Portland cement mixed with microsilica and barite matrixes. *J. Nucl. Mater.* **2011**, *415*, 132–137. [CrossRef]

15. Nicu, M.; Ionascu, L.; Dragolici, F.; Neacsu, E. The influence of chemical composition of the secondary radioactive waste on cement matrix conditioning. In Proceedings of the Energy and Clean Technologies Conference Proceedings, SGEM 2016, Vienna, Austria, 2–5 November 2016; Volume I, pp. 49–55, ISBN 978-619-7105-63-6.
16. Kononenko, O.A.; Milyutin, V.V.; Nekrasova, N.A. Composite binders for solidification of spent ion-exchange resins. *At. Energy* **2019**, *125*, 257–261. [CrossRef]
17. Kononenko, O.A.; Milyutin, V.V.; Makarenkov, V.I.; Kozlitin, E.A. Immobilization of NPP evaporator bottom high salt-bearing liquid radioactive waste into struvite-based phosphate matrices. *J. Hazard. Mater.* **2021**, *416*, 125902. [CrossRef]
18. Shi, C.J.; Jimenez, A.F.; Palomo, A. New cements for the 21st century: The pursuit of an alternative to Portland cement. *Cem. Concr. Res.* **2011**, *41*, 750–763. [CrossRef]
19. Luz, C.A.; Rocha, J.C.; Cheriaf, M.; Pera, J. Valorization of galvanic sludge in sulfoaluminate cement. *Constr. Build. Mater.* **2009**, *23*, 595–601. [CrossRef]
20. Zhu, J.P.; Chen, Y.; Zhang, L.; Guo, B.K.; Fan, G.X.; Guan, X.M.; Zhao, R.Q. Revealing the doping mechanism of barium in sulfoaluminate cement clinker phases. *J. Clean. Prod.* **2021**, *295*, 126405. [CrossRef]
21. Shi, C.; Spence, R. Designing of cement-based formula for solidification/stabilization of hazardous, radioactive, and mixed wastes. *Crit. Rev. Environ. Sci. Technol.* **2004**, *34*, 391–417. [CrossRef]
22. Zhang, W.; Wang, J. Leaching performance of uranium from the cement solidified matrices containing spent radioactive organic solvent. *Ann. Nucl. Energy* **2017**, *101*, 31–35. [CrossRef]
23. Sun, Q.N.; Hu, J.; Wang, J.L. Optimization of composite admixtures used in cementation formula for radioactive evaporator concentrates. *Prog. Nucl. Energy* **2014**, *70*, 1–5. [CrossRef]
24. Li, J.F.; Wang, J.L. Solidification of 30% TBP-OK Waste by calcium sulfoaluminate cement. *Adv. Mater. Res.* **2013**, *726–731*, 2782–2785. [CrossRef]
25. Li, J.F.; Wang, J.L. Advances in cement solidification technology for waste radioactive ion exchancre resins: A review. *J. Hazard. Mater.* **2006**, *135*, 443–448. [CrossRef]
26. Sun, Q.N.; Li, J.F.; Wang, J.L. Solidification of borate radioactive resins using sulfoaluminate cement blending with zeolite. *Nucl. Eng. Des.* **2011**, *241*, 5308–5315. [CrossRef]
27. He, C.; Osbaeck, B.; Makovicky, E. Pozzolanic reactions of six principal clay minerals: Activation, reactivity assessments and technological effects. *Cem. Concr. Res.* **1995**, *25*, 1691–1702. [CrossRef]
28. Murat, M.; Comel, C. Hydration reaction and hardening of calcined clays and related minerals III. Influence of calcination process of kaolinite on mechanical strengths of hardened metakaolinite. *Cem. Concr. Res.* **1983**, *13*, 631–637. [CrossRef]
29. Fernandez, R.; Martirena, F.; Scrivener, K.L. The origin of the pozzolanic activity of calcined clay minerals: A comparison between kaolinite, illite and montmorillonite. *Cem. Concr. Res.* **2011**, *41*, 113–122. [CrossRef]
30. Asteris, P.G.; Lourenco, P.B.; Roussis, P.C.; Adami, C.E.; Armaghani, D.J.; Cavaleri, L.; Chalioris, C.E.; Hajihassani, M.; Lemonis, M.E.; Mohammed, A.S.; et al. Revealing the nature of metakaolin-based concrete materials using artificial intelligence techniques. *Constr. Build. Mater.* **2022**, *322*, 126500. [CrossRef]
31. Antoni, M.; Rossen, J.; Martirena, F.; Scrivener, K. Cement substitution by a combination of metakaolin and limestone. *Cem. Concr. Res.* **2012**, *42*, 1579–1589. [CrossRef]
32. Bilal, H.; Chen, T.F.; Ren, M.; Gao, X.J.; Su, A.S. Influence of silica fume, metakaolin & SBR latex on strength and durability performance of pervious concrete. *Constr. Build. Mater.* **2021**, *275*, 122124. [CrossRef]
33. Nergis, D.D.; Vizureanu, P.; Sandu, A.V.; Nergis, D.P.; Bejinariu, C. XRD and TG-DTA study of new phosphate-based geopolymers with coal ash or metakaolin as aluminosilicate source and mine tailings addition. *Materials* **2022**, *15*, 202. [CrossRef] [PubMed]
34. Sabir, B.; Wild, S.; Bai, J. Metakaolin and calcined clays as pozzolans for concrete: A review. *Cem. Concr. Compos.* **2001**, *23*, 441–454. [CrossRef]
35. Zhang, P.; Wang, K.X.; Wang, J.; Guo, J.J.; Ling, Y.F. Macroscopic and microscopic analyses on mechanical performance of metakaolin/fly ash based geopolymer mortar. *J. Clean. Prod.* **2021**, *294*, 126193. [CrossRef]
36. Abdel Rahman, R.O.; Zin El Abidin, D.; Abou-Shady, H. Cesium binding and leaching from single and binary contaminant cement–bentonite matrices. *Chem. Eng. J.* **2014**, *245*, 276–287. [CrossRef]
37. Li, Z.P.; Lu, D.G.; Gao, X.J. Optimization of mixture proportions by statistical experimental design using response surface method—A review. *J. Build. Eng.* **2021**, *36*, 102101. [CrossRef]
38. Menchaca-Mendez, A.; Zapotecas-Martinez, S.; Garcia-Velazquez, L.M.; Coello, C.A. Uniform mixture design via evolutionary multi-objective optimization. *Swarm Evol. Comput.* **2022**, *68*, 100979. [CrossRef]
39. Wang, H.Y.; Zhang, C.Q. The mixture design threshold accepting algorithm for generating D-optimal designs of the mixture models. *Metrika* **2022**, *85*, 345–371. [CrossRef]
40. Scheffé, H. Experiments with mixtures. *J. R. Stat. Soc. Ser. B Methodol.* **1958**, *20*, 344–360. [CrossRef]
41. DeRousseau, M.A.; Kasprzyk, J.; Srubar, W.V. Computational design optimization of concrete mixtures: A review. *Cem. Concr. Res.* **2018**, *109*, 42–53. [CrossRef]
42. Zhang, W.; Li, J.; Wang, J. Solidification of spent radioactive organic solvent by sulfoaluminate and Portland cements. *J. Nucl. Sci. Technol.* **2015**, *52*, 1362–1368. [CrossRef]
43. Matsuzawa, K.; Atarashi, D.; Miyauchi, M.; Sakai, E. Interactions between fluoride ions and cement paste containing superplasticizer. *Cem. Concr. Res.* **2017**, *91*, 33–38. [CrossRef]

44. Liu, Y.; Li, H.; Wang, K.; Wu, H.; Cui, B. Effects of accelerator–water reducer admixture on performance of cemented paste backfill. *Constr. Build. Mater.* **2020**, *242*, 118187. [CrossRef]
45. Khaskhoussi, A.; Calabrese, L.; Bouhamed, H.; Kamoun, A.; Proverbio, E.; Bouaziz, J. Mixture design approach to optimize the performance of TiO_2 modified zirconia/alumina sintered ceramics. *Mater. Des.* **2018**, *137*, 1–8. [CrossRef]
46. Rahman, R.A.; Ojovan, M.I. Toward sustainable cementitious radioactive waste forms: Immobilization of problematic operational wastes. *Sustainability* **2021**, *13*, 11992. [CrossRef]
47. Helton, J.C.; Hansen, C.W.; Swift, P.N. Performance assessment for the proposed high-level radioactive waste repository at Yucca Mountain, Nevada. *Reliab. Eng. Syst. Saf.* **2014**, *122*, 1–6. [CrossRef]
48. Wang, J. Progress of geological disposal of high-level radioactive waste in China in the 21st century. *At. Energy Sci. Technol.* **2019**, *53*, 2072–2082.
49. Yu, X.; Ni, S.; Wang, Y.; Cai, G.; Xu, D. Experimental research on top cover of shallow-buried radioactive waste disposal repository. *Chin. J. Rock Mech. Eng.* **2009**, *28*, 1169–1176.
50. Li, J.W.; Xu, D.; Wang, W.L.; Wang, X.J.; Mao, Y.P.; Zhang, C.; Jiang, W.; Wu, C.L. Review on selection and experiment method of commonly studied simulated radionuclides in researches of nuclear waste solidification. *Sci. Technol. Nucl. Install.* **2020**, *2020*, 3287320. [CrossRef]
51. Alby, D.; Charnay, C.; Heran, M.; Prelot, B.; Zajac, J. Recent developments in nanostructured inorganic materials for sorption of cesium and strontium: Synthesis and shaping, sorption capacity, mechanisms, and selectivity—A review. *J. Hazard. Mater.* **2018**, *344*, 511–530. [CrossRef]
52. Xu, X.; Bi, H.; Yu, Y.; Fu, X.; Wang, S.; Liu, Y.; Hou, P.; Cheng, X. Low leaching characteristics and encapsulation mechanism of Cs+ and Sr2+ from SAC matrix with radioactive IER. *J. Nucl. Mater.* **2021**, *544*, 152701. [CrossRef]
53. Qian, G.R.; Shi, J.; Cao, Y.L.; Xu, Y.F.; Chui, P.C. Properties of MSW fly ash-calcium sulfoaluminate cement matrix and stabilization/solidification on heavy metals. *J. Hazard. Mater.* **2008**, *152*, 196–203. [CrossRef]
54. Shi, H.; Wu, Q.Y.; Yu, Z.Q.; Ma, J.; Shen, X.D. Properties of eco-friendly coral sand powder—Calcium sulfoaluminate cement binary system. *Construct. Build. Mater.* **2020**, *263*, 120181. [CrossRef]
55. Shi, J.Y.; Liu, B.J.; Tan, J.X.; Dai, J.D.; Chen, J.Z.; Ji, R.J. Experimental studies and microstructure analysis for rapid-hardening cement emulsified asphalt mortar. *J. Constr. Eng. Manag.* **2020**, *146*, 04020130. [CrossRef]
56. Wang, W.L.; Luo, Z.Y.; Shi, Z.L.; Cen, K.F. Experimental study on cement clinker co-generation in pulverized coal combustion boilers of power plants. *Waste Manag. Res.* **2006**, *24*, 207–214. [CrossRef] [PubMed]